

1 **Revised version #2**

2 **Experimental vs. natural fulgurite: a comparison and implications for the formation**
3 **process**

4
5 A. Zeynep Çalışkanoglu^{a,*}, Corrado Cimarelli^a, Donald B. Dingwell^a, Alessandra S. B.
6 Camara^b

7
8 ^aDepartment of Earth and Environmental Sciences, Ludwig-Maximilians-Universität,
9 Theresienstraße 41, 80333 Munich, Germany

10 ^bInstitute of Energy Systems Munich, Universität der Bundeswehr, Werner-Heisenberg-Weg
11 39, 85577 Neubiberg, Germany

12
13 *Corresponding author's E-mail address: zeynep.caliskanoglu@min.uni-muenchen.de

14
15 **Abstract**

16 Fulgurites are glassy structures formed when lightning strikes the ground, causing
17 ground material (e.g., rocks, sediments, or soil) to melt and fuse. While fulgurites are relatively
18 rare, they provide valuable insights into paleoecology and may play a key role in prebiotic
19 chemistry. Despite their significance in nature, understanding the conditions underlying the
20 formation of fulgurites poses severe challenges, as the physical parameters and timing of the
21 fulgurite-generating lightning event still need to be discovered.

22 Here, we use a unique opportunity from the recent *in situ* discovery of a natural fulgurite
23 still embedded in its protolith. Using a high voltage setup, we further compare this natural
24 fulgurite with the experimentally generated fulgurite obtained from the original protolith. The
25 natural and experimental fulgurites exhibit evidence of similar melting sequences and post-

26 melting recrystallization structures. Using Raman spectroscopy applied to the quartz phase
27 transition, we estimate the thermal gradient present in the fulgurite during formation to be a
28 minimum of 1600°C at the inner wall of the fulgurite and ca. 600°C at the outer wall of the
29 fulgurite. The natural fulgurite-generating event is also accessible via World Wide Lightning
30 Network data. Those findings suggest that the current responsible for the cloud-to-ground
31 lightning discharges that generated the natural fulgurite lay in the range of 11.960 kA to 14.473
32 kA. The state of the experimental fulgurites matched that of the natural fulgurite, validating the
33 experimental option for studying fulgurite generation.

34

35 Keywords: Fulgurite, Lightning discharge, Experiment, WWLLN, ENTLN

36

INTRODUCTION

37 Fulgurites are irregular, glassy, tube-shaped formations that occur when lightning
38 discharges (specifically cloud-to-ground or CG) melt the Earth's surface at peak temperatures,
39 followed by rapid cooling. They typically contain a large glass fraction hosting some initial
40 unmelted lithologies and often exhibit some quench crystallization.

41 Only one-third of thundercloud lightning discharges are estimated to reach the ground,
42 potentially generating fulgurites (Rakov 2016). Despite the limited number of examples, it has
43 been proposed that fulgurites may offer valuable data for paleoecology reconstructions
44 (Navarro-González et al., 2007; Ballhaus et al., 2017) and demonstrate the existence of rare
45 essential prebiotic chemical reactants, such as phosphite (e.g., Pasek and Block, 2009; Hess et
46 al., 2021; Çalışkanoğlu et al., 2023a; Bindi et al., 2023).

47 Previous fulgurite research has predominantly focused on natural examples (e.g., Pasek et
48 al., 2012; Ende et al., 2012; Stefeno et al., 2020; Karadag et al., 2022), with very few
49 experimental studies to date (e.g., Castro et al., 2020; Genareau et al., 2017). Those pioneering
50 experimental studies were severely limited in their ability to mimic natural lightning due to
51 constraints arising from technical aspects of the experiments, such as the absence of a trigger
52 or a continuing current. They, therefore, largely fail to replicate accurately the conditions of
53 fulgurite petrogenesis. In contrast, the high current and voltage experimental setup (see detail
54 in Çalışkanoğlu et al., 2023b) employed here enables the accurate simulation of lightning
55 discharges responsible for fulgurite formation.

56 Here, we compare a natural fulgurite (Eastern Türkiye) and an equivalent experimentally
57 generated fulgurite obtained using the *in situ* adjacent protolith as a starting material. The
58 experimental fulgurite, generated under variable well-controlled experimental conditions,
59 yields new insights into the textural evolution of the natural fulgurite and about temperature
60 gradients during melting and recrystallization at high cooling rates. Simultaneously, we report

61 the first detailed measurements of lightning discharge parameters that we infer led to the
62 formation of the natural fulgurite, thereby effectively constraining the electrical conditions
63 necessary for fulgurite formation.

64

65

MATERIAL AND METHODS

66 **The natural fulgurite**

67 A sample of natural fulgurite and its adjacent protolith were obtained from a private seller
68 who discovered the fulgurite in north-west Van-Türkiye ($38^{\circ}13'17.6''\text{N } 44^{\circ}15'55.9''\text{E}$) in mid-
69 April 2021 (Fig. 1a,b) after a thunderstorm of April 1st, 2021. The investigated natural fulgurite
70 part will be detailed in the Result section. The CG lightning associated with that thunderstorm
71 has been detected by radio-frequency antennas of Earth Networks Total Lightning Network
72 (ENTLN; Zhu et al., 2022). In addition to the approximate location of the lightning discharge,
73 the antennas provide the magnitude of the current associated with each lightning event. This
74 discovery provides us with a unique opportunity to evaluate natural fulgurite formation versus
75 experimental fulgurite formation from the protolith using independent control of lightning
76 parameters under realistic conditions.

77

78 **The target (protolith) material**

79 The protolith (a soil-bearing epiclastic sediment), collected from an area immediately
80 adjacent to the natural fulgurite (Fig. 1a), was used as a target material for the fulgurite
81 synthesis experiments. The remote location means no nearby communication poles might have
82 accidentally generated the fulgurites “artificially” (e.g., Kassi et al., 2013).

83 The local geology consists of several geological units from oldest to youngest: 1) pre-
84 Neogene pyroclastic deposits (pumice, tuff, and ignimbrites) and intermediate
85 (andesite/trachyandesite) deposits from Mount Yiğit (Türkecan 2017), 2) Neogene clastic

86 rocks (conglomerate, sandstone, marl, and - locally - tuff and lava blocks), 3) Pliocene
87 sedimentary deposits (Şenel et al., 1984) and basaltic lava flows, which represent the latest
88 stage of Mount Yiğit volcanism (1.87 ± 0.07 My; Allen et al., 2011). The protolith used as
89 experimental target material was collected from where the Neogene clastic rocks crop out (Fig.
90 2a).

91 The protolith appears yellowish-brown and is composed of rock fragments of varying sizes,
92 ranging from ca. 30 μm to a few centimeters, consisting of mono- and polymineralic grains.
93 The rock fragments exhibit sub-rounded to rounded edges. Energy-dispersive X-ray
94 spectroscopy (EDS) analysis reveals that the monomineralic grains include quartz, plagioclase,
95 and alkali feldspar, along with minor Fe- and Ti-oxides (Fig. 2b,c,d). The polymineralic grains
96 exhibit diverse compositions, but plagioclase, quartz, and alkali feldspar are the most common
97 minerals, with minor hornblende, biotite, apatite, zircon, Fe- and Ti-oxides (Fig. 2d,e). Most
98 clasts are fully crystalline (Fig. 2e-g), but some exhibit up to 20% glass (Fig. 2h). Backscattered
99 Electron (BSE) images reveal no evidence of lightning-induced effects in the protolith used
100 subsequently as experimental target material.

101

102 **Sample preparation and analytical techniques**

103 The target material was thoroughly cleaned to remove any potential macroscopic organics
104 (plants). The most comprehensive possible range of macroscopically distinct clasts was
105 selected and roughly crushed to less than 10 mm, and a mixture of them was embedded in
106 epoxy for further analytical analyses.

107 Several 10 mm chips of fulgurites (both natural and experimental) were embedded in their
108 respective epoxy mounts for microtextural analyses.

109 The surfaces of further chips of both natural and experimental fulgurites were examined
110 using a Keyence 3D Laser Scanning Confocal Microscope (LSCM) VK-X1000 with a 5x

111 objective lens (WD 22.5) in the Department of Earth and Environmental Sciences at Ludwig-
112 Maximilians-Universität (LMU), Munich - Germany.

113 BSE images of the target material, natural and experimental fulgurite samples, were
114 collected using Scanning Electron Microscopy (SEM) at LMU - Munich with an accelerating
115 voltage of 20 kV under a low vacuum. Semi-quantitative chemical composition data collection
116 at the SEM was conducted through EDS using an Oxford Instrument Aztech software
117 (AztechEnergy Advanced EDS-System) on the natural fulgurite, its protolith, and the
118 experimental fulgurite.

119 We used the confocal HORIBA Jobin Yvon XploRa micro-Raman spectrometer at the
120 Mineralogical State Collection Munich (SNSB) to identify mineral phases. The instrument was
121 calibrated with a silica standard, and the spectra were acquired with a green Nd: YAG-Laser
122 (532 nm wavelength), focused through the 100LWD objective lens, with 0.9 μm laser spot
123 diameter. Grating of 1800T, a confocal hole of 300 μm , a slit of 100 μm , and an exposure time
124 of 30 s three times acquired were applied. The backscattered Raman radiation was collected
125 between 100 - 1500 cm^{-1} , with an error of $\pm 1.5 \text{ cm}^{-1}$, to include the low and high wavenumber
126 regions.

127

128 **Fulgurite synthesis experiments**

129 We simulated natural lightning discharges in the high voltage laboratory at Universität der
130 Bundeswehr (UniBw) in Germany, utilizing a DC source with a trigger-pulse setup to
131 synthesize a fulgurite. The setup was designed based on recommendations from the lightning
132 research community, such as the waveforms specified in IEC 62305 (International
133 Electrotechnical Commission [IEC] 2010) derived from studies of natural lightning
134 phenomena. For further details regarding the experimental methodology and schematic
135 diagram of the setup, please refer to Çalışkanoglu et al. (2023b).

136 The lightning strikes are conducted between two electrodes placed inside a cylindrical
137 sample container, which is connected to an electrical apparatus consisting of two parts: a Marx
138 generator (which produced the trigger pulse) and a DC source (which acted as a prolonged
139 current generator). The container was filled with approximately 250 g of target material.
140 Initially, the Marx generator generated ca. 135 kA for ca. 100 microseconds, creating a
141 conductive path between the electrodes, which were 5.7 cm apart. This high voltage and current
142 initiated the melting of the target material. Subsequently, the DC source was kept constant
143 between ca. 280 and ca. 320 A for ca. 500 milliseconds, simulating the long duration of a
144 natural lightning discharge (Rakov and Uman, 2003; Lapierre et al., 2014). This prolonged
145 current promoted the melting of more material and facilitated the formation of a fulguritic mass.

146 Several experimental trials were conducted to establish the setup conditions and
147 comprehend the material's behavior under high current and voltage conditions. All experiments
148 were carried out at atmospheric temperature and pressure. In the first experiment, the target
149 material was utilized in its natural form (fragments ranging from 32 μm to a few cm), but no
150 melted pieces or fulguritic structures were observed. Simulated lightning is characterized by a
151 lower peak current than natural lightning, thus preventing larger grains from melting. To
152 ameliorate this discrepancy, ca. 50% of the coarse fraction ($> 10 \text{ mm}$) was removed, and the
153 experiment was repeated under the same electrical parameters as above, resulting in the
154 formation of a fulgurite. The waveform of the experimental current was recorded using a
155 Measurement Impulse Analyzer System (MIAS) at an 800-1000 ms time interval.

156

157 **Field lightning monitoring**

158 ENTLN comprises more than 1800 sensors deployed across more than 100 countries, which
159 detect broad-spectrum electric field signals originating from intracloud (IC) and CG lightning
160 events (Liu and Heckman, 2011). The CG lightning data is obtained from the World Wide

161 Lightning Location Network (WWLLN) to enhance ENTLN detection capabilities. The
162 WWLLN detects, locates, and timestamps lightning strikes worldwide with a spatial accuracy
163 of 10 km and a temporal accuracy of 10 μ s (Abreu et al., 2010; Holzworth et al., 2019; Hutchins
164 et al., 2012, 2013; Rodger et al., 2004, 2005). We utilized WWLLN data to identify natural
165 lightning events, which might have generated our natural fulgurite.

166 We focused on the period of April 1-15, 2021. Our search area was limited to an 8 km
167 radius around the location where the natural fulgurite was found. We detected one IC and two
168 CG lightning events (CG-1 and -2) within the focused area and time frame by using ENTLN
169 data (Table 1 and Fig. 1a). IC events do not generate fulgurite; thus, the IC data is neglected in
170 the present study. Both CG-1 and CG-2 lightning strokes showed a “downward negative”
171 direction (the most common for global CG lightning, Rakov and Uman (2003)). The CGs were
172 ordered according to the time of occurrence, with the location estimates CG-1 and CG-2
173 illustrated in Fig. 1a. It should be noted that due to the technical limitations of the antenna
174 network, the designated locations of the CGs are, within error, equivalent to the fulgurite
175 location (i.e., WWLLN - Rodger et al. (2005); ENTLN - Zhu et al. (2022)). Considering the
176 data from the WWLLN, we propose that one of these occurrences generated the investigated
177 natural fulgurite.

178

179 RESULTS

180 Natural fulgurite

181 The natural fulgurite is ca. 112 cm long and ca. 105 cm wide (Fig. 1b). It displays several
182 small branches connected to two main branches. An available piece of this fulgurite was
183 obtained commercially and investigated in the present study (Fig. 3a,b). Hereafter, we refer to
184 this sample as the “natural fulgurite”. The natural fulgurite is ca. 17 cm in length and has a
185 diameter of ca. 6 cm. It appears darker than the protolith. The outer surface of the natural

186 fulgurite has a rough texture with several unmelted grains remaining from the protolith (Fig.
187 2a). In contrast, the central portion of the natural fulgurite is entirely glassy. Vesicles of variable
188 shapes and sizes are present. The “main void” is the largest vesicle (ca. 2.5 cm in size) in the
189 natural fulgurite, as shown in Fig. 3b. Immediately adjacent to the glassy region is a zone of
190 large vesicle concentration. Smaller vesicles are distributed from the glassy region to the
191 unmelted protolith. (Fig. 3c). The fulgurite wall thickness varies from ca. 1 cm to 3 cm. The
192 fulgurite contains unmelted to partially-melted, angular, and sub-angular grains (up to a few
193 millimeters) and a fully-melted glassy region. Unmelted grains are common on the outer wall
194 of the fulgurite, whereas partially melted grains are typically scattered in the glassy mass. BSE
195 images show no sharp transition between unmelted and partially-melted grains. The glassy
196 mass is composed of a heterogeneous mingling of molten materials (Fig. 3d).

197 Natural fulgurite grains are mono- and polymineralic, occurring in unmelted and partially-
198 melted states. Monomineralic grains are typically alkali feldspar, plagioclase, and quartz or
199 minor Fe- and Ti-oxides. Melts apparently derived from feldspar mingle with the matrix-
200 derived melts, as evidenced by heterogeneity in the glass, in the form of flow structures (Fig.
201 3d). Partially-melted quartz crystals are commonly fractured (Fig. 3e). The phase change from
202 alpha (α) quartz (crystals located in the outer zone of the fulgurite) to cristobalite (crystals
203 located close to the inner wall) was also detected.

204 Post-melting recrystallization structures with different compositions were detected, as
205 shown in Table 2. No orientation is apparent in the growth pattern of these structures. Their
206 size reaches a maximum of 1 mm. Prismatic-tabular structures are observed, which are enriched
207 in SiO₂, Al₂O₃, CaO, and Na₂O (Fig. 3f). Skeletal structures are observed, which are enriched
208 in MgO (Fig. 3g). Other structures (i.e., cross, spherical and another skeletal) have notably high
209 FeO contents (Fig. 4a-c). The cross and spherical structures are found in proximity to one
210 another and appear to be formed sequentially. These structures' considerably smaller size (<1

211 μm) prevents accurate composition measurements because of SiO_2 and Al_2O_3 contamination
212 from the surrounding material. However, their compositions appear similar to those of the Fe-
213 containing phases.

214 The polymineralic grains in the natural fulgurite consist mainly of quartz, plagioclase,
215 and alkali feldspar, with minor biotite, hornblende, apatite, zircon, and oxides (Fe and Ti).
216 These grains are found in both unmelted and partially-melted regions. The volume fraction of
217 unmelted grains is much lower than that of partially-melted grains in the glassy region. Feldspar
218 crystals exhibit three morphologies: “solid,” “vesiculated”, and “molten”. The solid
219 morphology represents the feldspar crystals (either alkali feldspar or plagioclase) that do not
220 show any chemical and physical changes (i.e., unmelted) (Fig. 4d). These crystals are only
221 found in the outer wall of the natural fulgurite. The vesiculated morphology indicates crystals
222 containing mainly rounded vesicles (Fig. 4e). They are mostly found in the middle of the
223 natural fulgurite wall. The chemical composition of this region is enriched in SiO_2 , Al_2O_3 ,
224 Na_2O , and K_2O . The Na_2O and K_2O values are variable depending on the volume ratio of
225 plagioclase and alkali feldspar in the primary grains. The molten morphology may result from
226 feldspar crystals melting completely in the presence of some other minor phases, such as Fe-
227 oxide (Fig. 4f).

228

229 **Experimental fulgurite**

230 The experimentally-generated fulgurite is also tube-like without branches (Fig. 5a) and
231 appears dark brown. It is approximately 7 cm in length and 1 cm in width, with a main void
232 diameter of approximately 7 mm (Fig. 5b). The thickness of the fulgurite wall is ca. 2 mm. The
233 distribution of unmelted and partially-melted grains, as well as the glassy region, is found to
234 be quite similar to that of the natural fulgurite, and there is no sharp transition between
235 unmelted and partially-melted grains at the outer edge of the experimental fulgurite. However,

236 the proportion of the unmelted grains in the glassy region is much lower than in the natural
237 fulgurite, presumably due to the finer grain size of the target material. The average grain size
238 of both the unmelted and partially-melted grains is approximately 0.5 mm. Several vesicles,
239 ranging up to 1 mm in size (rounded and sub-rounded), are highly concentrated between
240 unmelted and partially-melted regions (Fig. 5c).

241 The experimental fulgurite contains mono- and polymineralic grains in both unmelted
242 and partially-melted forms. Quartz and feldspar crystals are the two monomineralic grains.
243 Feldspar crystals are mingled in the glassy region, resulting in the flow structures observed
244 (Fig. 5d). Quartz crystals are ca. 0.5 mm in size (Fig. 5e), and they exhibit physical deformation
245 such as fractures (Fig. 5f) and have been identified as α -quartz via Raman spectroscopic
246 analysis.

247 Three distinct post-melting recrystallization structures are observed. They are
248 numbered 1, 2, and 3 based on their structural differences from right to left on a BSE image
249 (Fig. 5g). They exhibit strong FeO enrichment together with high SiO₂ and Al₂O₃ contents
250 (Table 3). Structure 1 displays a cross-formed shape, as observed in the natural fulgurite (Fig.
251 4a). In structure 2, radial arms extend from a central point to form spherulites. Structure 3
252 displays a symmetric skeletal form. The structures 1 and 3 cover a larger area of the fulgurite
253 than the structure 2. Analysis of these small Fe-rich suffers from contamination (i.e., SiO₂ and
254 Al₂O₃) originating from the surrounding glass.

255 The polymineralic grains consist mainly of quartz, plagioclase, and alkali feldspar.
256 Hornblende, apatite, and minor Fe and Ti. These minor phases are solely detected in the
257 partially melted grains near the outer wall of the experimental fulgurite. Quartz crystals have
258 retained their general form with numerous fractures and show no notable chemical changes. In
259 contrast, feldspars exhibit chemical and mechanical changes. They show the same textural
260 morphologies (solid, vesiculated, molten) (Fig. 5h-j) as described for the natural fulgurite (Fig.

261 4d-f). Feldspar crystals (alkali feldspar and plagioclase) in the solid morphology are detected
262 in the outer wall of the experimental fulgurite (Fig. 5h). They exhibit enhanced vesiculation
263 (Fig. 5i). In the molten morphology, feldspars appear entirely molten without any recognizable
264 morphological crystal form close to the interior fulgurite wall, and they are surrounded by
265 fractured quartz crystals (Fig. 5j). EDS measurements on the well-mixed glassy region indicate
266 that the glass composition of the experimental fulgurite is quite similar to that of the natural
267 fulgurite (Table 2).

268

269

DISCUSSION

270 Fulgurite was experimentally generated from the protolith recovered adjacent to a natural
271 fulgurite. The formation of a fulgurite is confirmed to be a complex process that depends on
272 several factors, including the lightning parameters (i.e., temperature and current), as well as the
273 composition and the state of the host rock. Even though the current intensities of the natural
274 lightning discharge, ca. $13.000 \text{ kA} \pm 1.250$ (Table 1), and the experiment, ca. 300 A are vastly
275 different, our results reveal that the fulgurites generated in nature and experiments resemble
276 each other closely. A notable exception is that the higher natural current does lead to a higher
277 degree of melting of coarser grains. A possible explanation for this scale-invariant character
278 may lie in the intrinsic fractal nature of lightning discharges (Niemayer et al., 1984; Wiesmann
279 and Zeller, 1986). Previous work from Çalışkanoğlu et al. (2023b) indicates that the continuing
280 current of a lightning strike has a noticeable effect on the formation of fulgurite, indicating a
281 threshold of ca. 100 ms for fulgurite formation. We confirm here that a 300 A current and a
282 prolonged duration of discharge (ca. 100 ms) facilitates the formation of fulgurite from the
283 silicate protolith (Maurer 2021), as it has been previously demonstrated for non-silicate
284 (Çalışkanoğlu et al. 2023a) protolith.

285 Temperature gradients and grain size distribution both exert first-order influences on
286 fulgurite texture. The temperature of natural lightning discharges typically ranges between
287 10.000 to 28.000 K (Paxton et al., 1986). Based on melting temperatures, we observe that our
288 simulated lightning discharge generates a minimum of ca. 2000 K (Çalışkanoglu et al., 2023a-
289 b). Regions experiencing lower temperatures, due to their distal location to the lightning plasma
290 and higher concentration of coarse grain sizes, exhibit a higher proportion of partially-melted
291 and unmelted grains in the fulgurite, yielding distinct regions whose textures are systematically
292 defined by their degrees of melting (e.g., Hess et al., 2021; Kenny and Pasek, 2021;
293 Çalışkanoglu et al., 2023a-b). In both nature and experiment, coarse grains that have been
294 partially melted exhibit distinctive flow structures in their glassy products, indicating that such
295 melts are not homogenized during fulgurite formation (c.f. Lavallée et al., 2015). In contrast,
296 the homogeneous glassy (fully remelted) regions of experimental and natural fulgurites exhibit
297 similar chemistry as determined by SEM/EDS (Table 2).

298 Quartz crystals (initially both mono- and polymineralic grains) undergo a phase change
299 (Fig. 6a,b) with increasing temperature, resulting in a fractured structure. Folstad et al. (2023)
300 indicate that cracks in quartz are commonly observed in two temperature ranges. The first
301 range, approximately 300-600°C, primarily arises from volume changes in impurity regions,
302 uneven surfaces of quartz, and/or the presence of fluid inclusions. The second range, ca. 1300-
303 1600°C, is likely a consequence of the phase transformation of quartz from β -quartz to β -
304 cristobalite. As noted above, the natural fulgurite exhibits α -quartz in the outer wall and β -
305 cristobalite in the inner wall. This implies the presence of a strong temperature gradient across
306 ca. 1 cm. In contrast, the experimental fulgurite exhibits no cristobalite. Possible reasons for
307 this discrepancy include (1) the simulated lightning may not have reached the equivalent
308 temperature range and/or (2) the pressure generated by simulated lightning may be lower.

309 Feldspar crystals situated in proximity to the lightning plasma undergo complete melting,
310 whereas those subjected to lower temperatures display partial melting with vesicle formation.
311 This distinction within the feldspar crystals supports the strong temperature gradient extending
312 from the inner wall (adjacent to the plasma) to the outer wall of the fulgurite.

313 Upon cooling, both the natural and experimental fulgurites reveal the presence of multiple
314 coexisting crystalline structures (i.e., spherical and dendritic) (Fig. 3f-g, 4a-c and 5g). Similar
315 crystal structures have also been reported in other rapidly quenched glasses, such as impactites,
316 meteorites, and chondrules (e.g., Kumler and Day, 2021). Skeletal structure (magnetite) has
317 previously been documented in fulgurites by Ablesimov et al. (1986) and Grapes and Müller-
318 Sigmund (2010). To the best of our knowledge, this study marks the first documented
319 occurrence of spherical Fe-rich forms within natural and experimental fulgurites. The
320 juxtaposition of distinct growth patterns and crystal sizes might reflect locally varying melt
321 compositions and/or different cooling rates determined by proximity to the lightning plasma
322 and heterogeneous composition.

323

324

IMPLICATIONS

325 This work demonstrated a realistic comparison between natural and experimental fulgurites
326 for the first time, revealing a remarkable similarity in their textural and mineralogical evolution.
327 This validates that the state of the experimental fulgurite matched that of the natural fulgurite
328 using the DC source trigger-pulse setup as a lightning simulator. This work also further
329 documents the physical parameters (maximum voltage and current) of lightning strikes that
330 likely generated the natural fulgurite. Our results interestingly suggest a scale-invariant
331 character of the experimental fulgurites concerning the natural one, whereby the lower voltage
332 and current values used in the experiments allow the reproduction of identical textures observed
333 in the natural fulgurite. As shown in previous experiments, we confirm the importance of long-

334 duration (100's ms) continuous currents in favoring extensive melting and, ultimately, the
335 fulgurite formation. This work introduces a novel methodology for reproducible fulgurite
336 generation through laboratory experiments. This opens up possibilities for systematic
337 petrogenetic analysis of fulgurite formation with broader geological implications, providing
338 researchers with a controlled environment to explore and understand the processes involved.

339

340

ACKNOWLEDGMENTS

341 The research was financially supported by the Volkswagen Foundation (VW Stiftung)
342 under Project-ID 94809. DBD acknowledges ERC 2018 ADV Grant 834255 (EAVESDROP),
343 and CC acknowledges ERC 2019 COG Grant 864052 (VOLTA). The authors thank Dr. Jeff
344 Lapierre for providing the ENTLN dataset. The authors thank Prof. Dr. Philippe Schmitt-
345 Kopplin for his assistance and technical support and Prof. Dr. Daniel Weidendorfer for useful
346 discussions and advice. They would like to thank Associated Editor Kate Kiseeva for her
347 careful guidance and two reviewers (Christopher J. Stefano and an anonymous) for their
348 thorough reviews.

349

350

REFERENCE CITED

351 Ablesimov, N.Y., Tsyurupa, A.I., and Lipatov, V.G. (1986) Phase and element ratios upon
352 fulguritization of basalt. *Trans (Dokl) USSR Acad. Scientific Earth Science Section*
353 290, 161–164.

354 Abreu, S.F., Chandan, D., Holzworth, R.H., and Strong, K. (2010) A performance assessment
355 of the World Wide Lightning Location Network (WWLLN) via comparison with the
356 Canadian Lightning Detection Network (CLDN). *Atmospheric Measurement*
357 *Techniques*, 3, 1143–1153, <https://doi.org/10.5194/amt-3-1143-2010>.

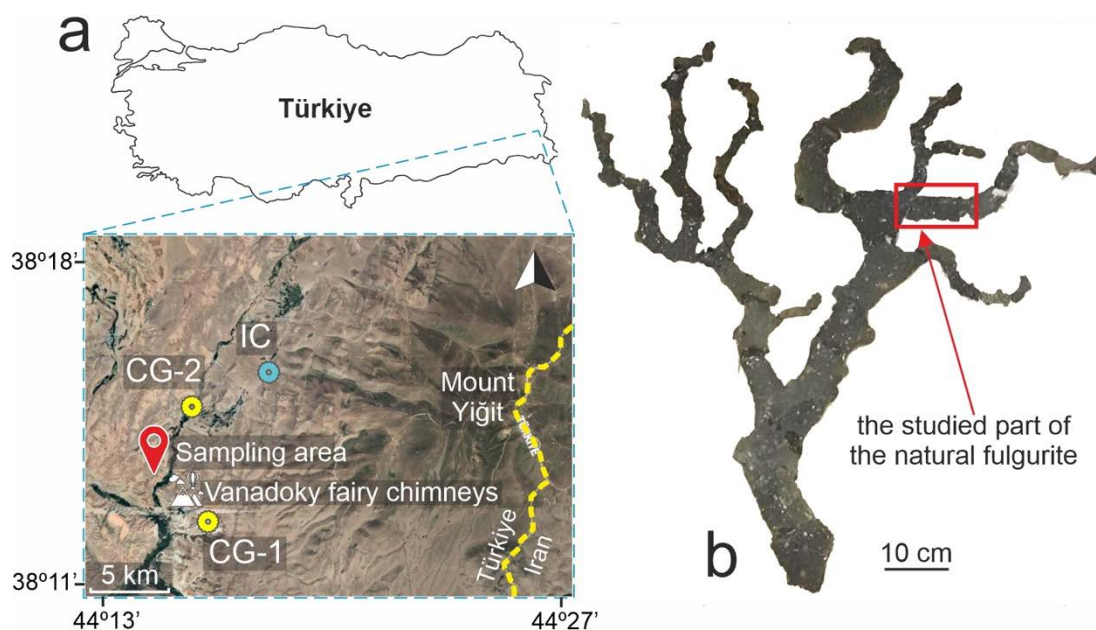
- 358 Allen, B.M., Mark, F.D., Kheirkhah, M., Barfod, D., Emami, H. M., and Saville, C. (2011)
359 $^{40}\text{Ar}/^{39}\text{Ar}$ dating of Quaternary lavas in northwest Iran: constraints on the landscape
360 evolution and incision rates of the Turkish–Iranian plateau. *Geophysical Journal*
361 *International*, 1–14, <https://doi.org/10.1111/j.1365-246X.2011.05022.x>.
- 362 Ballhaus, C., Wirth, R., Fonseca, R.O.C., Blanchard, H., Pröl, W., Bragagni, A., Nagel, T.,
363 Schreiber, A., Dittrich, S., Thome, V. et al. (2017) Ultra-high pressure and ultra-
364 reduced minerals in ophiolites may form by lightning strikes. *Geochemical Perspectives*
365 *Letters*, 5, 42-46, <https://doi.org/10.7185/geochemlet.1744>.
- 366 Bindi, L., Feng, T., and Pasek, M.A. (2023) Routes to reduction of phosphate by high-energy
367 events. *Communication Earth & Environments*, 4, 70, [https://doi.org/10.1038/s43247-](https://doi.org/10.1038/s43247-023-00736-2)
368 [023-00736-2](https://doi.org/10.1038/s43247-023-00736-2).
- 369 Castro, J.M., Keller, F., Feisel, Y., Lanari, P., Helo, C., Mueller, S.P., Schipper, C.I., and
370 Thomas, C. (2020) Lightning-induced weathering of Cascadian volcanic peaks. *Earth*
371 *Planet Science Letters*, 552, 116595, <https://doi.org/10.1016/j.epsl.2020.116595>.
- 372 Çalışkanoğlu, A.Z., Dingwell, D.B., Cimarelli, C., Camara, A.S.B., Breitzke, H.,
373 Buntkowsky, G., Pasek, M.A., Braun, D., Scheu, B., and Molaverdikhani, K. (2023a)
374 Reactive phosphorus via simulated lightning discharge: A role for fulgurites in pre-
375 biotic chemistry. *Chemical Geology*, 620, 121343,
376 <https://doi.org/10.1016/j.chemgeo.2023.121343>.
- 377 Çalışkanoğlu, A.Z., Camara, A.S.B., Cimarelli, C., Dingwell, D.B., and Hess, K.U. (2023b)
378 Experimental generation of fulgurite under realistic lightning discharge conditions.
379 *Scientific Reports*, 13, 11685, <https://doi.org/10.1038/s41598-023-38781-8>.
- 380 Ende, M., Schorr, S., Kloess, G., Franz, A., and Tovar, M. (2012) Shocked quartz in Sahara
381 fulgurite. *European Journal of Mineralogy*, 24, 499-507, [https://doi.org/10.1127/0935-](https://doi.org/10.1127/0935-1221/2012/0024-2188)
382 [1221/2012/0024-2188](https://doi.org/10.1127/0935-1221/2012/0024-2188).

- 383 Folstad, M.A., Yu, H., Wang, H., and Tangstad, M. (2023) Disintegration of six different
384 quartz types during heating to 1600 °C. *Minerals*, 13, 132, [https://doi.org/10.3390/](https://doi.org/10.3390/min13020132)
385 [min13020132](https://doi.org/10.3390/min13020132).
- 386 Genareau, K., Gharghabi, P., Gafford, J., and Mazzola, M. (2017) The elusive evidence of
387 volcanic lightning. *Scientific Reports*, 7, 1–9, [https://doi.org/10.1038/s41598-017-](https://doi.org/10.1038/s41598-017-15643-8)
388 [15643-8](https://doi.org/10.1038/s41598-017-15643-8).
- 389 Grapes, R.H., and Müller-Sigmund, H. (2010) Lightning-strike fusion of gabbro and
390 formation of magnetite-bearing fulgurite, Cornone di Blumone, Adamello, Western
391 Alps, Italy. *Mineralogy and Petrology*, 99, 67-74, [https://doi.org/10.1007/s00710-009-](https://doi.org/10.1007/s00710-009-0100-3)
392 [0100-3](https://doi.org/10.1007/s00710-009-0100-3).
- 393 Hess, B.L., Piazzolo, S., and Harvey, J. (2021) Lightning strikes as a major facilitator of
394 prebiotic phosphorus reduction on early Earth. *Nature Communications*, 12, 1535,
395 <https://doi.org/10.1038/s41467-021-21849-2>.
- 396 Holzworth, R.H., McCarthy, M.P., Brundell, J.B., Jacobson, A.R., and Rodger, C.J. (2019)
397 Global distribution of superbolts. *Journal of Geophysical Research: Atmospheres*, 124,
398 9996-10005, <https://doi.org/10.1029/2019JD030975>.
- 399 Hutchins, M.L., Holtzworth, R.H., Rodger, C.J., and Brundell, J.B. (2012) Far-field power of
400 lightning strokes as measured by the World Wide Lightning Location Network. *Journal*
401 *of Atmospheric and Oceanic technology*, 29, 1102-1110, [https://doi.org/10.1175/jtech-](https://doi.org/10.1175/jtech-d-11-00174.1)
402 [d-11-00174.1](https://doi.org/10.1175/jtech-d-11-00174.1).
- 403 Hutchins, M.L., Jacobson, A.R., Holzworth, R.H., and Brundell, J.B. (2013) Azimuthal
404 dependence of VLF propagation. *Journal of Geophysical Research: Space Physics*, 118,
405 5808-5812, <https://doi.org/10.1002/jgra.50533>.
- 406 International Electrotechnical Commission (IEC). (2010) Protection against lightning - Part
407 1: General Principles (2nd ed.), ISBN 978-2-88912-280-6.

- 408 Karadag, A., Kaygisiz, E., Nikitin, T., Ongen, S., Ogruc Ildiz, G., Aysal, N., Yilmaz, A., and
409 Fausto, R. (2022) Micro-Raman Spectroscopy and X-ray Diffraction Analyses of the
410 Core and Shell Compartments of an Iron-Rich Fulgurite. *Molecules*, 27, 3053,
411 <https://doi.org/10.3390/molecules27103053>.
- 412 Kassi, A.M., Kasi A.K., Friis, H., and Kakar, D.M. (2013) Occurrences of rock fulgurites
413 associated with steel pylons of the overhead electric transmission line at Tor Zawar,
414 Ziarat District and Jang Tor Ghar, Muslim Bagh, Pakistan. *Turkish Journal of Earth
415 Science*, 22, 1010-19, <https://doi.org/10.3906/yer-1207-6>.
- 416 Kenny, G.G., and Pasek, M.A. (2021) The response of zircon to the extreme pressures and
417 temperatures of a lightning strike. *Scientific Reports*, 11, 1560,
418 <https://doi.org/10.1038/s41598-021-81043-8>.
- 419 Kumler, B., and Day, J.M.D. (2021) Trace element variations generated by magmatic and
420 post-crystallization processes in eucrite meteorites. *Geochimica et Cosmochimica Acta*,
421 301, 211-229, <https://doi.org/10.1016/j.gca.2021.03.002>.
- 422 Lapierre, J.L., Sonnenfeld, R.G., Edens, H.E., and Stock, M. (2014) On the relationship
423 between continuing current and positive leader growth. *Journal of Geophysical
424 Research: Atmospheres*, 119, 12-479, <https://doi.org/10.1002/2014JD022080>.
- 425 Lavallée, Y., Hirose, T., Kendrick, J.E., Hess, K.U., and Dingwell, D.B. (2015) Fault
426 rheology beyond frictional melting. *Proceedings of the National Academy of
427 Sciences*, 112(30), 9276-9280, <https://doi.org/10.1073/pnas.1413608112>.
- 428 Liu, C., and Heckman, S. (2011) The application of total lightning detection and cell tracking
429 for severe weather prediction. In *Proceedings of the 91st American Meteorological
430 Society Annual Meeting*, Seattle, WA, USA, 23–27.

- 431 Maurer, B. (2021) Lightning induced olivine spherules. Experimental generation and
432 structural and chemical characterization of crystalline and glassy particles generated by
433 artificial lightning. [MS.c. Thesis]: Ludwig-Maximilians-Universität, 71.
- 434 Navarro-González, R., Mahan, S.A., Navarro-Aceves, R., Rajot, J.L., McKay, C.P., Coll, P.,
435 and Raulin, F. (2007) Paleoecology reconstruction from trapped gases in a fulgurite
436 from the late Pleistocene of the Libyan Desert. *Geology*, 35, 171-174,
437 <https://doi.org/10.1130/G23246A.1>.
- 438 Niemeyer, L., Pietrono, L. and Wiesmann H.J. (1984) Fractal dimension of dielectric
439 breakdown, *Physical Review Letters*, 52(12), 1033–1036,
440 [doi:10.1103/PhysRevLett.52.1033](https://doi.org/10.1103/PhysRevLett.52.1033).
- 441 Pasek, M.A., and Block, K. (2009) Lightning-induced reduction of phosphorus oxidation
442 state. *Nature Geoscience*, 2, 553-556, <http://dx.doi.org/10.1038/ngo580>.
- 443 Pasek, M. A., Block, K., and Pasek, V. (2012) Fulgurite morphology: a classification scheme
444 and clues to formation. *Contributions to Mineralogy and Petrology*, 164, 477-492,
445 <https://doi.org/10.1007/s00410-012-0753-5>.
- 446 Rakov, V.A. (2016) *Fundamentals of lightning*. Cambridge University Press.
- 447 Rakov, V.A., and Uman, M.A. (2003) *Lightning: physics and effects*. Cambridge University
448 Press.
- 449 Paxton, A.H., Gardner, R.L., and Baker, L. (1986) Lightning return stroke: a numerical
450 calculation of the optical radiation. *Lightning Electromagnetics*, 29, 2736-41.
- 451 Rodger, C.J., Brundell, J.B., Dowden, R.L., and Thomson, N.R. (2004) Location accuracy of
452 long distance VLF lightning location network. *Annales Geophysicae*, 22, 747-758,
453 <https://doi.org/10.5194/angeo-22-747-2004>.

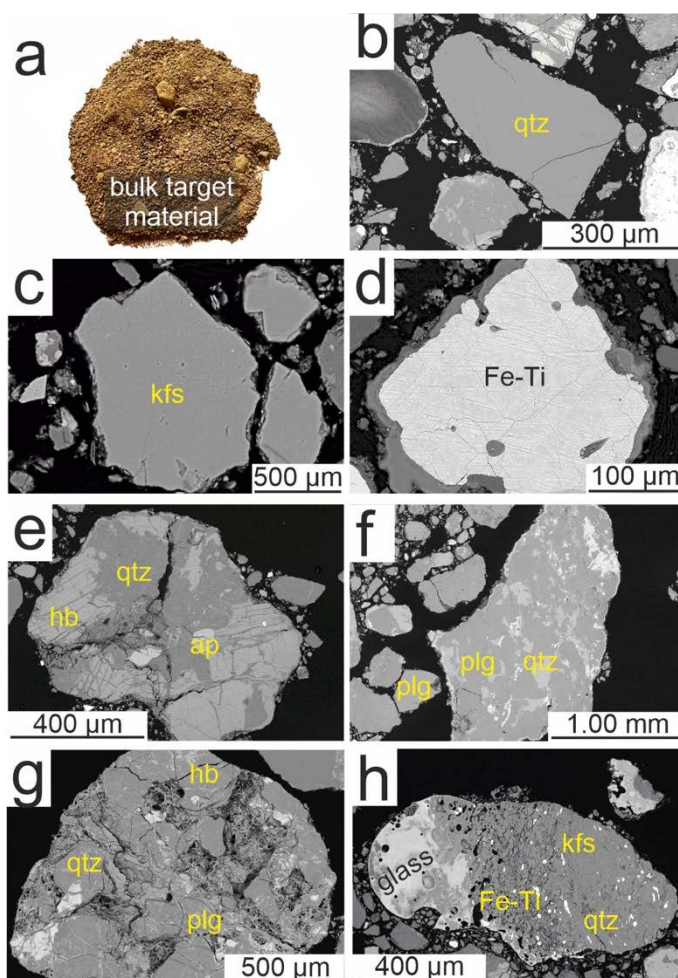
- 454 Rodger, C.J., Brundell, J.B., and Dowden, R.L. (2005) Location accuracy of VLF World
455 Wide Lightning Location (WWLL) network: Postalgorithm upgrade. *Annales*
456 *Geophysicae*, 23, 277-290, <https://doi.org/10.5194/angeo-23-277-2005>.
- 457 Stefano, C.J., Hackney, S.A., and Kampf, A.R. (2020) The occurrence of iron silicides in a
458 fulgurite: Implications for fulgurite genesis. *The Canadian Mineralogist*, 58, 115-123.
459 <https://doi.org/10.3749/canmin.1900019>.
- 460 Şenel, M., Acarlar, M., Çakmakoğlu, A., Dağar, Z., Erkanol, D., Örcen, S., Taşkıran, M.A.,
461 Ünal Ulu, M.F., and Yıldırım, H. (1984) Özalp (Van)-İran sınırı arasındaki alanın
462 jeolojisi. Maden Tetkik ve Arama Genel Müdürlüğü Rapor No: 7623, Ankara,
463 (unpublished).
- 464 Türkecan, A. (2017) İran sınırında bir volkan – Yiğit dağı. MTA Doğal Kaynaklar ve
465 Ekonomi Bülteni, 23, 77-86.
- 466 Wagstaff, F.E. (1969) Crystallization and Melting Kinetics of Cristobalite. *Journal of the*
467 *American Ceramic Society*, 52(12), 650-654, [https://doi.org/10.1111/j.1151-](https://doi.org/10.1111/j.1151-2916.1969.tb16069.x)
468 [2916.1969.tb16069.x](https://doi.org/10.1111/j.1151-2916.1969.tb16069.x).
- 469 Wiesmann, H.J. and Zeller, H.R. (1986) A fractal model of dielectric breakdown and pre-
470 breakdown in solid dielectrics. *Journal of Applied Physics*, 60 (5), 1770-1773,
471 <https://doi.org/10.1063/1.337219>.
- 472 Zhu, Y., Stock, M., Lapierre, J., and DiGangi, E. (2022) Upgrades of the Earth networks total
473 lightning network in 2021. *Remote sensing*, 14(9), 2209,
474 <https://doi.org/10.3390/rs14092209>.
- 475



476

477 **FIGURE 1.** Sampling area and general image of the natural fulgurite. (a) The fulgurite was
478 found northwest of the Vanadoky fairy chimneys in Van, Türkiye. The ENTLN detected two
479 CG and one intracloud (IC) lightning discharges. The topographic image is taken from Google
480 Maps (2023). (b) A photographic image of the natural fulgurite is shown. The red rectangle
481 indicates the portion of the natural fulgurite object of this study.

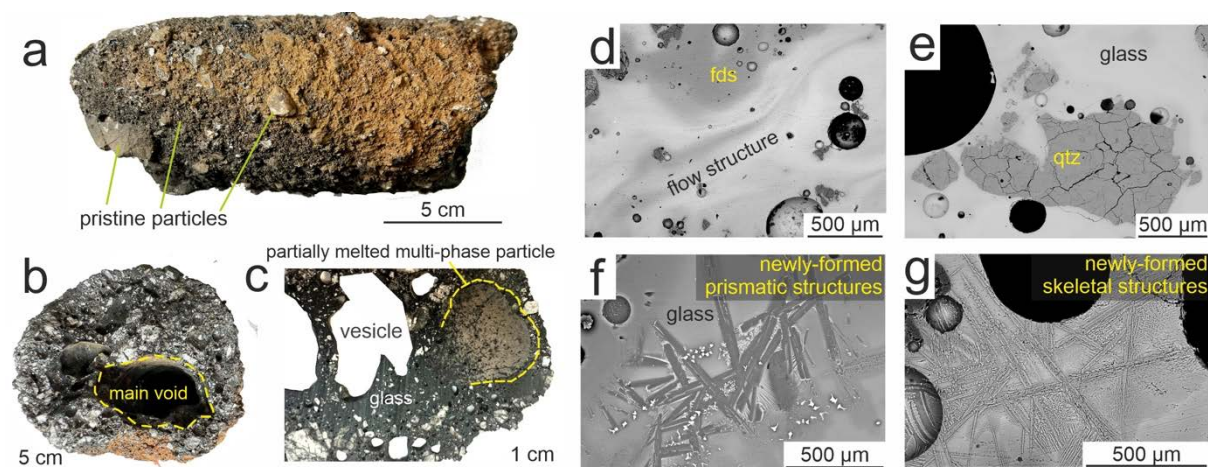
482



483

484 **FIGURE 2.** Target material and detailed BSE images of its heterogeneous grains. (a) An image
485 of the protolith of natural fulgurite. (b-f) Mono- and polymineralic grains of the target material.
486 These grains represent the sampling area's clastic rock unit (Şenel et al., 1984). Quartz: qtz,
487 Alkali feldspar: kfs, Oxides: Fe-Ti, Hornblende: hbl, Apatite: ap, Plagioclase: plg.

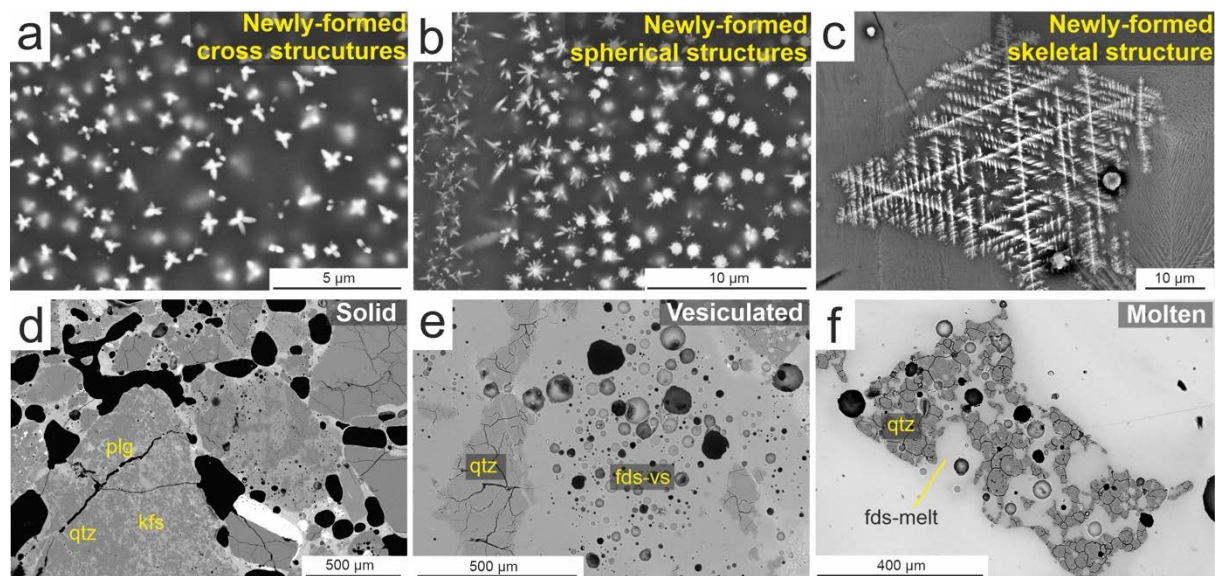
488



489

490 **FIGURE 3.** Detailed optical and BSE images of the natural fulgurite. (a) A photo of the studied
491 part of the fulgurite specimen in detail. (b) A section view of the natural fulgurite exhibits the
492 “main void”. (c) An optical image of a segment of a section of the natural fulgurite captured
493 by 3D LSCM, showing vesicles of varying sizes and shapes. (d) The heterogeneous glass mass
494 displays a flow structure within the glass mass. (e) BSE images reveal fractured quartz crystals.
495 (f) Newly-formed prismatic-tabular structures exhibit enrichment in SiO₂, Al₂O₃, Na₂O and
496 K₂O. (g) Newly-formed skeletal structures present MgO enrichment. Feldspar: fds.

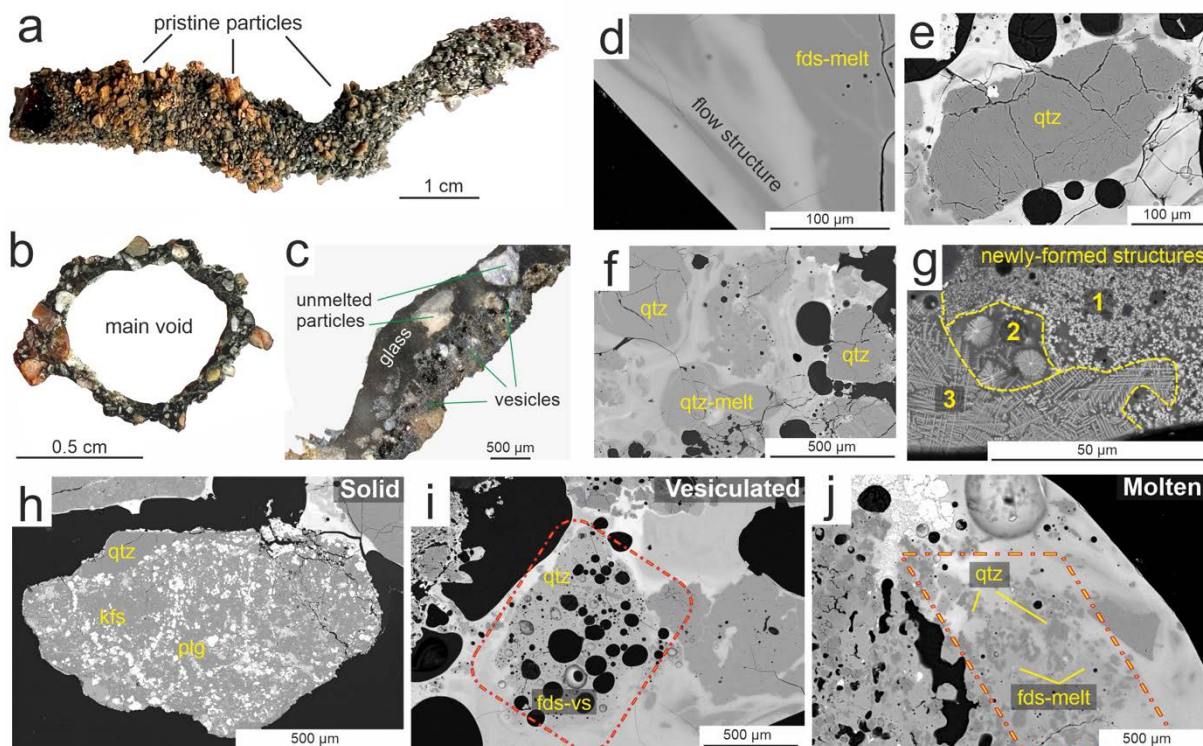
497



498

499 **FIGURE 4.** Post-melting recrystallization structures and melting morphologies of the main
500 crystals (feldspar) in the natural fulgurite are shown in (a-c) and (d-f), respectively. Fe-rich
501 recrystallization structures grew in different forms, such as cross (a), spherical (b), and skeletal
502 (c). (d) Unmelted polymineralic grains are named “solid”. (e) Feldspar displays vesicles due to
503 high-temperature interactions in the “vesiculated”. (f) The “molten” exhibits complete melting
504 of the feldspar. Vesicle: vs.

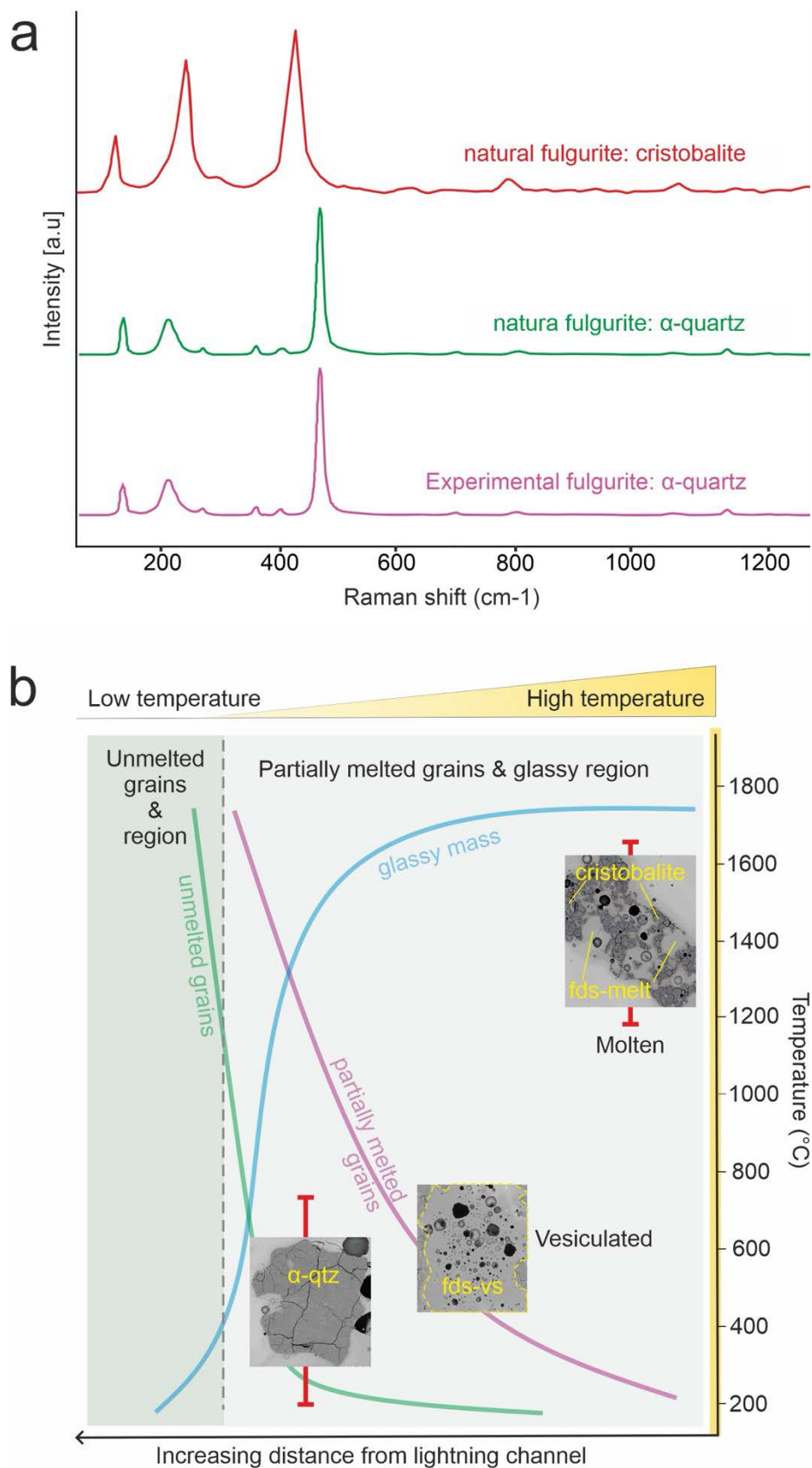
505



506

507 **FIGURE 5.** Optical and BSE images of the experimental fulgurite. (a) A photo of the
508 experimentally generated fulgurite. (b) A sectional view of the experimental fulgurite. (c) An
509 optical image of the fulgurite shows unmelted and partially-melted mono- and polymineralic
510 grains in a glassy mass. (d) Partially-melted feldspar crystals, which have mingled with the
511 glass mass. (e) A BSE image of a monomineralic partially-melted quartz. (f) Partially-melted
512 quartz and alkali feldspar crystals. (g) Newly formed structures grew in different forms (i.e.,
513 spherical and skeletal). The feldspar crystals exhibit a “solid” (h), “vesiculated” (i), and
514 “molten” morphologies (j) in the polymineralic grains.

515



516

517 **FIGURE 6.** Micro-Raman spectroscopy of quartz crystals and a schematic diagram illustrating

518 the evolution of grains in the fulgurites. (a) The Raman spectra of quartz crystals in fulgurites

519 from each fulgurite's inner and outer walls. The experimental fulgurite exhibits only α -quartz
520 and natural fulgurite displays both α -quartz and cristobalite. (b) The textural evolution of the
521 fulgurites concerning temperature development during lightning discharge. The textural
522 evolution among the defined morphologies (i.e., solid, vesiculated, and molten) is scaled in
523 temperature using the α - β transition (Folstad et al., 2023) and cristobalite stability (Wagstaff
524 1969).

525 **TABLE 1:** WWLLN data around the sampling area of the natural fulgurite.

Type of lightning	Date	Time	Location	Peak current [kA]	IC height [km]	Number sensors
IC	01.04.20	12:25:32	38°15'01.2"N 44°18'32.7"E	5.113	18.917	5
CG-1	01.04.20	17:27:14	38°11'04.6"N 44°17'19.3"E	-14.473	0	6
CG-2	01.04.20	17:29:41	38°14'22.2"N 44°16'47.3"E	-11.960	0	5

526

527 **TABLE 2.** Chemical composition of natural and experimental fulgurites (SEM-EDS
 528 normalized data).

Natural fulgurite										
	Glass mass	Melting morphologies of feldspar				Post-melting recrystallization structures				
		Solid		Vesiculated	Molten	Fe-rich phases			Prismatic -tabular	Mg-rich skeletal
		Plagioclase	Alkali feldspar			Cross	Spherical	Skeletal		
Si ₂ O	60.11	66.07	64.69	67.24	69.21	57.31	42.29	3.60	56.89	54.07
Al ₂ O ₃	17.01	21.45	18.82	20.76	17.41	13.50	11.45	2.12	25.94	4.89
FeO	9.91	0.17	0.14	0.19	2.99	22.92	35.21	91.23	2.14	12.76
CaO	3.29	1.85	0.06	0.69	1.95	0.78	0.81	0.01	8.63	2.22
K ₂ O	2.61	0.96	14.63	3.53	3.30	0.37	0.31	0.02	0.60	0.36
Na ₂ O	3.09	9.31	1.58	7.35	3.63	2.41	4.16	0.18	5.13	0.56
MgO	2.49	0.1	0.02	0.09	1.20	1.63	2.02	0.50	0.34	24.19
TiO ₂	1.26	0.04	0.02	0.03	0.24	1.01	3.15	1.86	0.22	0.47
MnO	0.19	0.02	0.01	0.03	nd	0.05	0.13	0.03	0.04	0.28
Cr ₂ O ₃	0.04	nd	0.02	0.02	nd	0.02	0.02	0.06	0.07	0.02
W	nd	Nd	nd	nd	nd	nd	0.45	0.19	nd	0.09
Cu	nd	0.03	0.01	nd	0.08	nd	nd	0.02	nd	nd

Experimental fulgurite										
	Glass mass	Melting morphologies of feldspar				Post-melting recrystallization structures				
		Solid		Vesiculated	Molten	Fe-rich phases			Structure 3	
		Plagioclase	Alkali feldspar			Structure 1	Structure 2			
Si ₂ O	64.11	65.48	63.77	66.07	63.98	21.53	21.61	42.07		
Al ₂ O ₃	17.78	21.87	18.89	19.14	24.42	nd	8.31	14.42		
FeO	6.71	0.92	0.24	2.35	0.38	77.13	65.26	31.52		
CaO	3.57	0.65	0.07	0.52	0.88	nd	1.26	1.73		
K ₂ O	1.91	1.94	16.68	8.05	2.82	0.07	0.42	1.94		
Na ₂ O	2.28	8.38	0.22	3.27	7.20	1.12	0.80	2.33		
MgO	1.52	0.31	0.08	0.5	0.16	nd	1.03	2.78		
TiO ₂	1.18	0.10	nd	nd	nd	0.04	1.04	2.98		
MnO	0.11	0.25	0.02	nd	0.39	nd	0.08	0.20		
Cr ₂ O ₃	nd	0.10	nd	nd	0.55	0.10	0.17	nd		
W	0.72	0.35	nd	nd	0.06	0.01	nd	nd		
Cu	nd	nd	0.03	0.01	0.10	nd	0.04	nd		

529